RSC Advances

PAPER

View Article Online
View Journal | View Issue

Cite this: *RSC Adv.*, 2025, **15**, 34399

On the generality of dye incorporation in silica nanoparticles

Qingwu Yao,†[ab] Yuying Yang,†[a] Xuejun Cheng,[bc] Huai Lin,[a] Xueyang Liu *[a] and Hongyu Chen [bc]

Received 27th May 2025
Accepted 19th August 2025

DOI: 10.1039/d5ra03724g

rsc.li/rsc-advances

Doping dyes in silica has a wide range of applications, but there is currently no general method of synthesis. Here, we show that 98 cationic dyes of 11 series could be directly doped in silica nanoparticles of uniform size. In this co-precipitation method, the negatively charged silica precursor, poly(silicic acid), basically wraps the dyes as counter ions and preserves them.

Introduction

Functionalized nanomaterials, as core research subjects in materials science, provide crucial support for breakthroughs in numerous key technologies. Among these, silica, a well-known inorganic nanomaterial, holds an important position owing to its unique physicochemical properties. Its synthesis methods are simple and controllable, and it demonstrates excellent performance such as catalytic degradation[1–3] and efficient adsorption[4–7] by virtue of its unique microporous structure. Most importantly, its favorable biocompatibility endows it with irreplaceable advantages in biomedical fields including drug delivery[8–11] and bioimaging.[12,13]

Composite materials formed by incorporating fluorescent dyes into silica nanoparticles (NPs) can impart stable luminescent properties to NPs, thereby enabling their application as tools such as fluorescent markers[14,15] and biological probes across multiple research fields. The realization of this stable luminescent characteristic is attributed to the effective protective effect of silica on fluorescent dyes: silica provides an ideal encapsulated microenvironment for them, which can effectively isolate interference from external factors (*e.g.*, light, oxidation).[16] This protective mechanism prevents dye molecules from losing efficacy due to environmental impacts, thereby ensuring the stability of their luminescent properties.

These characteristics collectively confer significant application potential upon fluorescent dye-silica nanoparticles. In the field of bioimaging,[13] their capacity to clearly label cells or tissues provides a powerful visualization tool for disease diagnosis and exploration of pathological mechanisms; in research on substance migration and transformation, they can function as high-sensitivity fluorescent labeling probes to achieve precise tracking;[15] in immunoassays,[17] by virtue of their specific binding with target molecules, these materials can also effectively enhance the accuracy and efficiency of detection.

Recently, we have shown that a rotor-based fluorophore, thioflavin T (ThT), can be embedded in silica NPs and serve as a reporter for changes in their solvent environment. As such, the solvent exchange into the NPs can be monitored by the stopped-flow technique with millisecond time resolution, to obtain the diffusion constants.[18]

Despite many efforts, the methods for doping dyes in silica still have obvious limitations, specifically manifested in their applicability often being restricted to specific conditions, such as specific dye types or reaction environments, and lacking universality. Therefore, developing effective strategies with strong universality remains an important challenge in the development of this field.

Currently, the main methods for doping dyes in silica can be divided into two categories: covalent coupling and physical encapsulation. The former involves directly bonding dyes to silane linking molecules, and the formed conjugates then undergo co-precipitation with silica. This method has specific requirements for the structure of dye molecules, requiring them to possess functional groups that can react with silanes, which to a certain extent limits the range of applicable dyes. In the latter method, cationic dyes are directly incorporated during the Stöber method[19] or microemulsion method.[20] Among them, the Stöber method is widely adopted due to its simple operation and easily controllable conditions, and its doping performance can be effectively improved through systematic dye screening.

We show in our previous studies that the silica synthesized in aqueous solution should be viewed as a highly swollen, cross-linked inorganic polymer, rather than a dense solid like glass or quartz: the precursor poly(silicic acid) is highly polar and

[a]*Institute of Advanced Synthesis, School of Chemistry and Molecular Engineering, Nanjing Tech University, Nanjing 211816, Jiangsu Province, China. E-mail: ias_xyliu@njtech.edu.cn*

[b]*Department of Chemistry, School of Science and Key Laboratory for Quantum Materials of Zhejiang Province, Research Center for Industries of the Future, Westlake University, Hangzhou 310030, P. R. China*

[c]*Institute of Natural Sciences, Westlake Institute for Advanced Study, Hangzhou 310024, China*

† These authors contributed equally to this work.

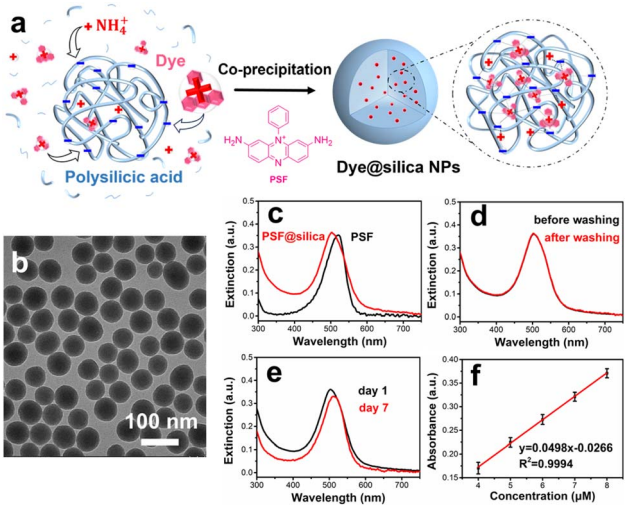

Fig. 1 (a) Schematics illustrating the co-precipitation of silica with doped dyes. (b) TEM image of the PSF@silica NPs. UV-vis extinction spectra of (c) PSF and PSF@silica NPs; (d) PSF@silica NPs before and after washing with ethanol; (e) PSF@silica NPs before and after storage in water at 4 °C for 7 days. (f) Standard curve for determining PSF's loading in silica.

carries multiple negative charges.[21,22] As such, its precipitation critically depends on the presence of counter ions and a bad solvent, such as the NH^{4+} ions and the water/ethanol mixture in the Stöber method. The preferential precipitation of long polymer chains and swelling by water explain the selective etching to make hollow NPs, the huge percentage of doped cations,and the intrinsic Fig. 1 micro-porosity of silica shells. As a result,we could modulate the silica etching to make multi-layered structures, exchange out the cations with H^+ to improve the cross-linking, and dope divalent Ca^{2+} ions to make silica readily etchable.[23]

On the basis of these understandings, we believe that there should be a general approach to incorporate cationic dyes in silica NPs, by simple co-precipitation without the hassle of chemical conjugation. Here, we show that among the 105 dyes we have collected, 98 could be directly incorporated in silica NPs (Fig. 2 and 3).

Experimental

Materials

All chemical reagents were used without further purification. The chemicals used are isopropanol (IPA, HPLC, Admas-beta), ammonia ($NH_3 \cdot H_2O$, 25–28% w/w, Shanghai Aladdin Biochemical Technology Co., Ltd), hydrochloric acid (HCl, 36.0–38.0% w/w, J&K Scientific Co., Ltd), tetraethyl orthosilicate (TEOS, 99%, J&K Scientific Co., Ltd), ethanol (ETOH, AR, Sinopharm Chemical Reagent Co., Ltd), Milli-Q water (resistivity 18.2 mΩ cm at 25 °C). The dyes are shown in Table S1.

Methods

Synthesis of silica nanoparticles

In 1.4 mL of water/IPA mixed solvent (water : IPA = 2 : 5), 15 μL of ammonia solution and 3 μL of TEOS were sequentially added, and then the mixture was stirred and reacted at 20 °C for 10 hours (in the dark). After the reaction, the product was centrifuged at 12 000 rpm for 12 minutes followed by a centrifugation-re-dispersion procedure with DI water. Finally, the product was redispersed in 1 mL DI water and stored in the refrigerator.

Synthesis of dye@silica nanoparticles

1 mg (phenosafranine) PSF was dissolved in 8.26 mL water/IPA mixed solvent (water : IPA = 2 : 5), and the dissolution of dyes was accelerated by ultrasonic treatment to prepare a homogenous PSF solution (0.3 mM). Then 15 μL of ammonia solution and 3 μL of TEOS were sequentially added into 1.4 mL the above PSF solution. The mixture was stirred and reacted at 20 °C for 10 hours (in the dark). After the reaction, the product was centrifuged at 12 000 rpm for 12 minutes. It was then purified once with 1 mL DI water. For the second purification, 5 μL of ethanol was added in 1 mL DI water, and for the third purification, 1 mL DI water was used. The supernatant after purification was confirmed to be free of unreacted PSF using UV-vis spectroscopy. Finally, the product was dispersed in 1 mL DI water and stored in the refrigerator.

Results and discussion

We first select 10-phenylphenazin-10-ium-2,8-diamine (phenosafranine, PSF), a dye in the phenazine family (Fig. 2e), for our model reaction: it was dissolved in a mixture solvent (water/IPA = 2 : 5) to obtain a red solution. Then, $NH_3 \cdot H_2O$ and tetraethyl orthosilicate (TEOS) were added, and the resulting reaction mixture was stirred for 10 h (Fig. 1a). Here, $NH_3 \cdot H_2O$ is used to promote the hydrolysis of the silica precursor TEOS, and IPA reduces the solvent polarity to promote silica precipitation. After the reaction is complete, the product silica NPs were isolated by centrifugation to give a red precipitate, which were re-dispersed in water (defined as 1 washing cycle). After 2 more washing cycles, the final supernatant was colourless, and the precipitate remained red, indicating that PSF has been successfully incorporated in the silica NPs (PSF@silica). In transmission electron microscopy (TEM) images, they are highly monodispersed nanospheres, with uniform diameters of 58.0 ± 7.3 nm (a survey of 300 NPs, Fig. 1b and S1). ·In addition, our synthesis method also features high reproducibility. The repeated syntheses are labeled as a, b, and c respectively, and the products obtained from these repeated experiments still exhibit highly similar chemical properties (Fig. S2).

The UV-vis peak of the PSF@silica NPs occurs at 510 nm, which is blue-shifted from the 520 nm peak of PSF in water (Fig. 1c). It is likely due to the higher refractive index of silica (1.45) than that of water (1.33). As calculated from the standard curve (Fig. 1f), in this study, the dye loading is defined as the number of nanomoles of PSF doped per micromole of TEOS during the synthesis process. The results showed that 2.1% of the initial dye was successfully incorporated, corresponding to a dye loading of 0.68 nmol PSF per μmol TEOS, with a synthesis cost of approximately 0.015 $ per nmol.

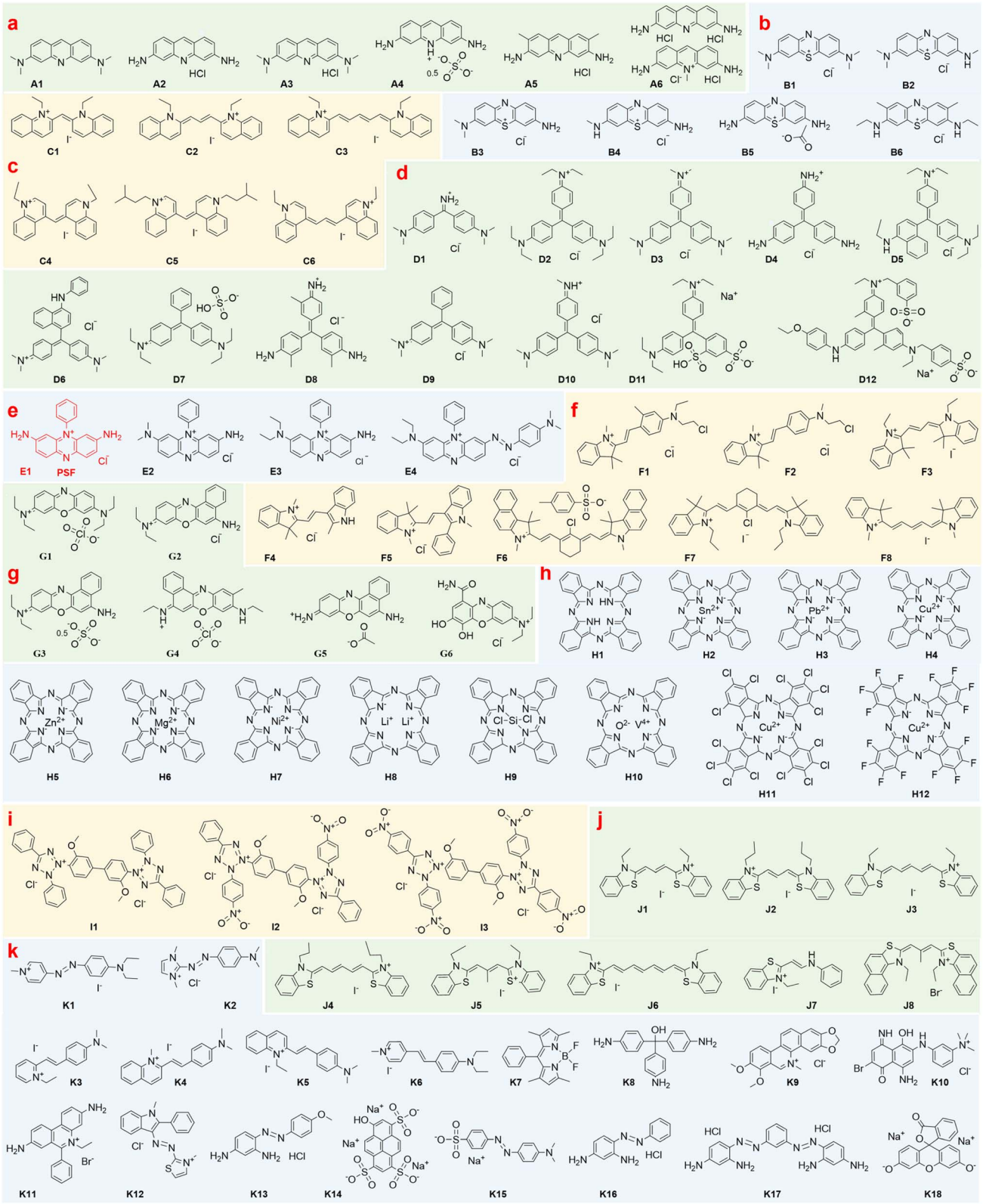

Fig. 2 Molecular structure of the dyes. (a) Acridine series dyes; (b) phenothiazine series dyes; (c) takagawa series dyes; (d) arylmethane series dyes; (e) phenazin series dyes; (f) indole series dyes; (g) phenoxazine series dyes; (h) phthalocyanine series dyes; (i) tetrazolium series dyes; (j) benzothiazole series dyes; and (k) other dyes.

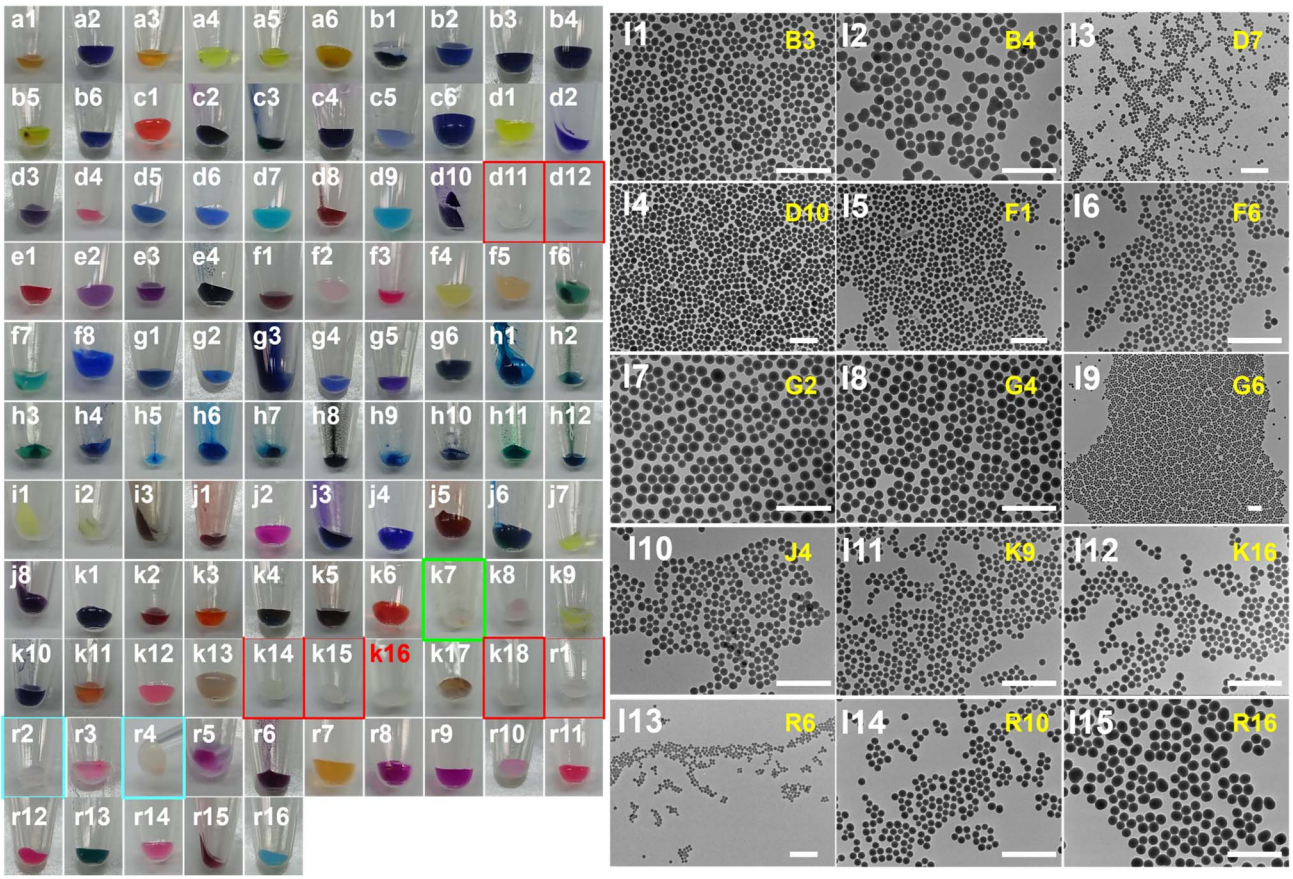

Fig. 3 Photos of all the dyes used in this work after co-precipitation with silica. (a1–6) acridine series dyes. (b1–6) phenothiazine series dyes. (c1–6) takagawa series dyes. (d1–12) arylmethane series dyes. (e1–4) phenazin series dyes. (f1–8) indole series dyes. (g1–6) phenoxazine series dyes. (h1–12) phthalocyanine series dyes. (i1–3) tetrazolium series dyes. (j1–8) benzothiazole series dyes. (k1–18) other dyes. (r1–16) oxanthene dyes. (l1–l15) TEM images of the dye@silica nanoparticles prepared with co-precipitation method. Bar: 200 nm.

PSF has good solubility in ethanol, and thus, we used a small amount of ethanol (5 μL) to remove any dyes that may adsorb on the NP surface, followed by dispersing the PSF@silica NPs in 1 mL of water. After an additional washing cycle with water to remove the residual ethanol, the final precipitate remained roughly the same colour intensity (Fig. 1d), indicating that most of the PSF was inside the silica domain. The PSF@silica NPs were stored at 4 °C for 7 days and then washed with water. The UV-vis extinction was essentially unchanged, indicating that PSF has not been dissolved by water (Fig. 1e).

When the initial [PSF] concentration increased from 0.10 to 0.30, 0.50, and 0.70 mM, the PSF loading increased from 0.20 to 0.68, 0.96, and 1.28 nmol PSF per μmol TEOS, respectively, and the particle size of the product PSF@silica also increased (Table S2). It is worth noting that when the concentration of [PSF] was increased to 0.50 mM, obvious silicon precipitation was observed after standing for 24 hours (Fig. S3a and b). Moreover, with the increase of dye doping concentration in silica nanoparticles, the transmission electron microscopy characterization results showed that the morphology of the particles gradually changed from uniform spheres to fused spheres (Fig. S3c–e), indicating that a higher loading amount led to a decrease in the stability of the silica nanoparticles. Therefore, we usually use a relatively low dye concentration (0.3 mM, unless otherwise specified).

As introduced, our previous work embedded the rotor-type fluorescent molecule thioflavin T (ThT) into silica nanoparticles. By monitoring fluorescence intensity changes during solvent exchange, we characterized solvent diffusion in silica and inferred corresponding porosity changes.[18] The research showed that more embedded ThT correlated with lower solvent diffusion, *i.e.*, lower silica porosity. Extending this understanding of silica pores to the current work, higher PSF doping concentrations in silica correspond to lower porosity.

Three additional dyes in the phenazine family, named as E2–E4 (Fig. 2e), were also successfully loaded in silica NPs. The resulting NPs were monodispersed nanospheres (Fig. S4), have intense colours corresponding to that of the respective dyes, and are also stable against washing cycles with water. A notable difference is that the loading amount of E4 was 18 times higher than that of E1. Moreover, the particle size of E4@silica is about 400 nm, much larger than the corresponding NPs of E1–E3 (60–80 nm). We propose that strong binding between dye molecules and silica arises primarily from electrostatic interactions, with charge interactions playing a key role. Notably, previous studies confirm that dye embedding is spontaneous (*i.e.*, $\Delta G < 0$), and

the embedding amount depends primarily on two energy factors: the dye's solvation energy in the solvent (ΔG_{sol}) and its interaction with confined pores (ΔG_{int}).[24] When the latter exceeds the former in favorability, dye embedding is promoted. Specifically, E4 interacts more favorably with silica's confined pores than other dyes, enabling broader binding within these pores and thus a higher doping amount.

Zeta potential measurements showed that, comparing to the silica NPs (−1.19 mV), E1 and E2 incorporation did not greatly change the surface charges (2.27 and −2.54 mV, Fig. S5). For E3 and E4, the zeta potential decreased significantly (−18.13 and −34.24 mV), likely due to higher dye loading (Table S4).

More extensive studies showed that, unlike the phenazine family dyes E1–E4, many dyes underwent degradation during the synthesis. Take the arylmethane series dyes (D1–D12, Fig. 2d) as example, 10 of them were found to degrade in a simple basic solution (0.20 M ammonia in water), with D8 and D11 being the exception. D4, D7, D9 and D10 were almost completely degraded in 2 h, showing 89.8%, 100%, 100%, 72.9% decrease of the major extinction peak, respectively. After addition of HCl, 6 of the dyes (D1, D3, D4, D7, D9, D10) showed some degree of reversibility, and D5, D6, and D12 were fully reversible (Fig. S6 and Table S4). This phenomenon may be directly associated with the conjugated systems of dye molecules, such as arylmethane skeletons and azo bonds. Upon adding ammonia water, hydroxyl groups irreversibly disrupt these conjugated systems *via* nucleophilic attacks-including processes like dealkylation of tertiary amines-and hydrolysis of azo bonds, resulting in dye degradation. In contrast, when hydrochloric acid is added, the acidic environment allows some degradation products to reconstruct partial conjugated structures through protonation (for instance, amine groups re-engage in p–π conjugation after protonation), leading to partial recovery from dye degradation. Notably, dye degradation involves independent chemical mechanisms linked to molecular structure, so no further in-depth discussion is provided.

With the coprecipitation method, all of the positively charged dyes (D1–D10) were doped in silica NPs, and the negatively charged D11 and D12 were not (Fig. 3). Despite their chemical instability, the doped dye@silica were stable in the preparative solution (basic solution with 0.15 mM ammonia) without further colour loss, highlighting the protecting role of silica. The purified dye@silica were all stable when stored.

To investigate the effect of molecular charge, we picked the oxanthene family dyes (Fig. 4). Again, all of the positively charged dyes (R7–16) were doped in silica. Among the remaining amphoteric dyes, the sulfonate-containing R1 are clearly too negatively charged to be incorporated, and the R6 with reactive –NCS could be readily bonded to silica *via* chemical reaction. R2–R5 are less predictable: While they have similar molecular structure, R3 and R5 could be incorporated, R2 cannot, and R3 showed only slightly coloured silica with a minor extinction peak (Fig. S7). Most importantly, by direct comparison, once the –COOH group of R3, R4, R5 was esterified (Fig. 4b–d), the dye loading was dramatically improved.

We also attempted 9 additional series of dyes, including the acridine family dyes (A1–A6), the phenothiazine family (B1–B6), the takagawa family (C1–C6), the indole family (F1–F8), the phenoxazine family (G1–G6), the phthalocyanine family (H1–H12), the tetrazolium family (I1–I3), the benzothiazole family (J1–J8) and other dyes (K1–K18).

In total, there are 105 organic dyes, most of which contain partial positive charge. Among them, 98 have been incorporated and the products were mostly uniform nano-spheres. All of the molecules with obvious negative charge, such as those with –SO_3^- group (D11, D12, K14, K15, R1) and K18 with overall negative charge, cannot be incorporated. K7 is neutral and thus led to low doping. There are 2 amphoteric ones with no doping (R2) or low doping level (R4). K16 is an exception, that it carries

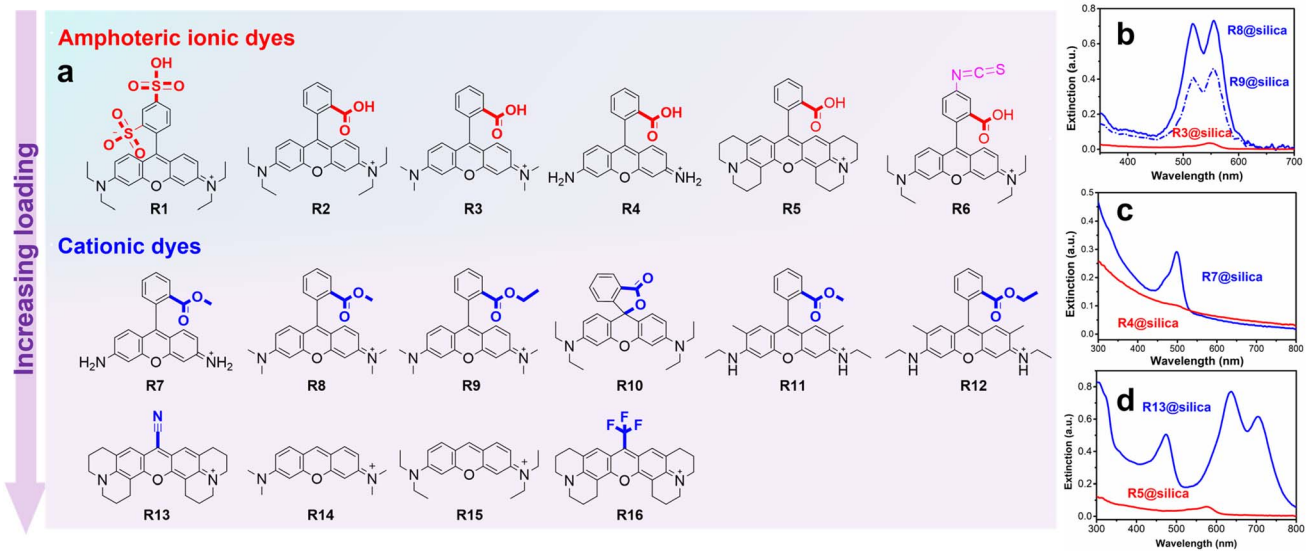

Fig. 4 (a) The oxanthene family dyes R1–16. Extinction spectra of (b) R3@silica, R8@silica and R9@silica, (c) R4@silica and R7@silica, (d) R5@silica and R16@silica, showing that esterification of the –COOH group makes a big difference in terms of dye loading.

positive charge but only has a low doping (Fig. S8). On these bases, charge interaction among the organic dyes and the silica precursor poly (silicic acid) is assigned as the dominant factor for the general synthesis.

Conclusions

In conclusion, we successfully embedded 98 dye molecules into silica nanoparticles *via* co-precipitation, clearly validating the reliability and universality of this one-pot synthesis strategy for preparing functionalized nanomaterials. This also reaffirms that silica-analogous to a negatively charged swollen polymer-forms efficient, stable nanostructures with positively charged ions through charge interactions. Future work will further expand the method's loading capacity for additional functional molecules (*e.g.*, biological probes and therapeutic drugs) and enable precise customization of the physicochemical properties of functionalized nanoparticles, thereby strongly supporting practical applications in related fields.

Author contributions

Q. Y. and Y. Y. contributed equally to this work. The manuscript was written through the contributions of all the authors. All authors have given approval to the final version of the manuscript.

Conflicts of interest

There are no conflicts to declare.

Data availability

The authors confirm that the data supporting the findings of this study are available within the article and the SI.

Supplementary information: relevant information of the dye molecules used in this paper, dye stability testing, zeta potential testing, UV-vis spectra, TEM images, and zeta potential graphs. See DOI: **https://doi.org/10.1039/d5ra03724g**.

Acknowledgements

We gratefully acknowledge the financial support from the National Natural Science Foundation of China: Major Research Plan (Project No. 92356310); Leading Innovative and Entrepreneur Team Introduction Program of Zhejiang (Project No. TD2022004) and Foundation of Westlake University. We thank Westlake university instrumentation and service center for molecular sciences for the facility support and technical assistance. We thank the Research Center for Industries of the Future (RCIF) at Westlake University for supporting this work.

References

1 Z. Yan, L. Fu, X. Zuo and H. Yang, Green assembly of stable and uniform silver nanoparticles on 2D silica nanosheets for catalytic reduction of 4-nitrophenol, *Appl. Catal., B*, 2018, **226**, 23–30.

2 N. Wang, X. Li, X. Lian, Q. Zhuang, J. Wang, J. Li, H. Qian, K. Miao, Y. Wang, X. Luo and G. Feng, Acetate Ions Facilitated Immobilization of Highly Dispersed Transition Metal Oxide Nanoclusters in Mesoporous Silica, *Inorg. Chem.*, 2024, **63**(9), 4393–4403.

3 C. Wang, W. Ma, T. Jia, X. Zhang and X. Fan, Label-free SERS-colorimetry dual-mode biosensor based on CRISPR/Cas12a triggered G-quadruplex capped magnetic meso-porous silica microspheres, *Sens. Actuators, B*, 2025, **422**, 136452.

4 E. Da'na, Adsorption of heavy metals on functionalized-mesoporous silica: A review, *Microporous Mesoporous Mater.*, 2017, **247**, 145–157.

5 S. Ijaz, A. Kausar, M. Iqbal, N. El Messaoudi, Y. Miyah, S. Knani and B. Graba, Advances in extraction of silica from rice husk and its modification for friendly environmental wastewater treatment *via* adsorption technology, *J. Water Proc. Eng.*, 2025, **71**, 107187.

6 H. Li, X. Chen, D. Shen, F. Wu, R. Pleixats and J. Pan, Functionalized silica nanoparticles: classification, synthetic approaches and recent advances in adsorption applications, *Nanoscale*, 2021, **13**(38), 15998–16016.

7 S. Liu, X. Chen, W. Ai and C. Wei, A new method to prepare mesoporous silica from coal gasification fine slag and its application in methylene blue adsorption, *J. Cleaner Prod.*, 2019, **212**, 1062–1071.

8 A. García-Fernández, F. Sancenón and R. Martínez-Máñez, Mesoporous silica nanoparticles for pulmonary drug delivery, *Adv. Drug Delivery Rev.*, 2021, **177**, 113953.

9 M. Manzano and M. Vallet-Regí, Mesoporous Silica Nanoparticles for Drug Delivery, *Adv. Funct. Mater.*, 2019, **30**(2), 1902634.

10 Y. Zhou, G. Quan, Q. Wu, X. Zhang, B. Niu, B. Wu, Y. Huang, X. Pan and C. Wu, Mesoporous silica nanoparticles for drug and gene delivery, *Acta Pharm. Sin. B*, 2018, **8**(2), 165–177.

11 N. Wang, W. Zhou, M. Yan, M. Zhang, H. Wang and H. Chen, Direct silica coating of drug crystals for ultra-high loading, *Nanoscale*, 2020, **12**(9), 5353–5358.

12 F.-F. An and X.-H. Zhang, Strategies for Preparing Albumin-based Nanoparticles for Multifunctional Bioimaging and Drug Delivery, *Theranostics*, 2017, **7**(15), 3667–3689.

13 Y. Wang, Q. Zhao, N. Han, L. Bai, J. Li, J. Liu, E. Che, L. Hu, Q. Zhang, T. Jiang and S. Wang, Mesoporous silica nanoparticles in drug delivery and biomedical applications, *Nanomed. Nanotechnol. Biol. Med.*, 2015, **11**(2), 313–327.

14 O. S. Wolfbeis, An overview of nanoparticles commonly used in fluorescent bioimaging, *Chem. Soc. Rev.*, 2015, **44**(14), 4743–4768.

15 J. S. D. Mieog, F. B. Achterberg, A. Zlitni, M. Hutteman, J. Burggraaf, R.-J. Swijnenburg, S. Gioux and A. L. Vahrmeijer, Fundamentals and developments in fluorescence-guided cancer surgery, *Nat. Rev. Clin. Oncol.*, 2021, **19**(1), 9–22.

16 L. Jin, X. Li, C. Liu and H. Pang, Nanoreactors derived from silica-protection-assisted metal-organic framework, *Chin. Chem. Lett.*, 2020, **31**(9), 2207–2210.
17 X. Wang, X. Li, A. Ito, Y. Watanabe, Y. Sogo, N. M. Tsuji and T. Ohno, Stimulation of *In Vivo* Antitumor Immunity with Hollow Mesoporous Silica Nanospheres, *Angew. Chem., Int. Ed.*, 2015, **55**(5), 1899–1903.
18 X. Cheng, Y. Pu, S. Ye, X. Xiao, X. Zhang and H. Chen, Measuring Solvent Exchange in Silica Nanoparticles with Rotor-Based Fluorophore, *Adv. Mater.*, 2023, **36**(3), 2305779.
19 P. P. Ghimire and M. Jaroniec, Renaissance of Stöber method for synthesis of colloidal particles: New developments and opportunities, *J. Colloid Interface Sci.*, 2021, **584**, 838–865.
20 X. Zhang and Y. Fan, Preparation of spherical silica particles in reverse micro emulsions using silicon tetrachloride as precursor, *J. Non-Cryst. Solids*, 2012, **358**(2), 337–341.
21 X. Song, T. Ding, L. Yao, M. Lin, R. L. Siew Tan, C. Liu, K. Sokol, L. Yu, X. W. Lou and H. Chen, On the Origin and Underappreciated Effects of Ion Doping in Silica, *Small*, 2015, **11**(34), 4351–4365.
22 Y. J. Wong, L. Zhu, W. S. Teo, Y. W. Tan, Y. Yang, C. Wang and H. Chen, Revisiting the Stöber Method: Inhomogeneity in Silica Shells, *J. Am. Chem. Soc.*, 2011, **133**(30), 11422–11425.
23 X. Cheng, J. Huang, R. Wang, Y. Xu, N. Wu, J. Zhou, X. Liu, H. Wang and H. Chen, Inorganic–organic coprecipitation: spontaneous formation of enclosed and porous silica compartments with enriched biopolymers, *Nanoscale*, 2023, **15**(5), 2394–2401.
24 X. Xiao, Q. Hong, X. Yan, R. Liu, Y. Wu, C. Li, B. Gu, G. He and H. Chen, Extreme Confinement Effects on the Incorporated Dyes in Metal–Organic Frameworks, *Aggregate*, 2025, e70093.